AD-A178 245 MECHANISM OF PHOTON-GATED PERSISTENT SPECTRAL HOLE-BURNING IN METAL-TETRA. (U) IBM ALMADEN RESEARCH CENTER SAN JOSE CA T P CARTER ET AL. 17 FEB 87 TR-11 1/1

UNCLASSIFIED N00014-84-C-0708 F/G 7/4 NL

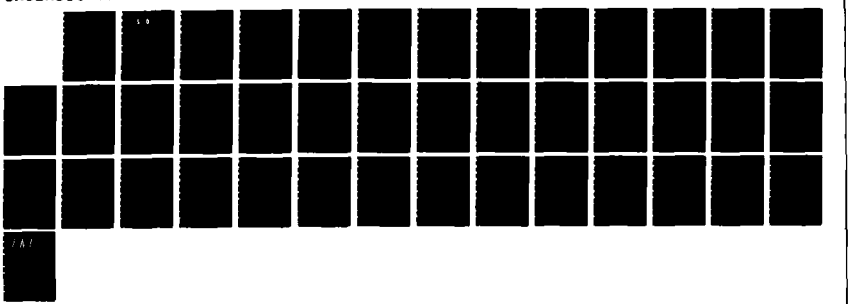

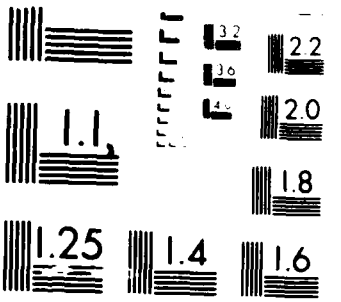

AT GOVERNMENT EXPENSE

(12)

AD-A178 245

SECURITY CLA

REPORT DOCUMENTATION PAGE

1a. REPORT SECURITY CLASSIFICATION: UNCLASSIFIED	1b. RESTRICTIVE MARKINGS
2a. SECURITY CLASSIFICATION AUTHORITY	3. DISTRIBUTION / AVAILABILITY OF REPORT
2b. DECLASSIFICATION / DOWNGRADING SCHEDULE	
4. PERFORMING ORGANIZATION REPORT NUMBER(S): Technical Report #11, IBM RJ 5506	5. MONITORING ORGANIZATION REPORT NUMBER(S)
6a. NAME OF PERFORMING ORGANIZATION: IBM Almaden Research Center; 6b. OFFICE SYMBOL (If applicable)	7a. NAME OF MONITORING ORGANIZATION: Office of Naval Research, Chemistry Div.
6c. ADDRESS (City, State, and ZIP Code): 650 Harry Road, San Jose, CA 95120-6099	7b. ADDRESS (City, State, and ZIP Code): Code 1113, Arlington, VA 22217
8a. NAME OF FUNDING / SPONSORING ORGANIZATION; 8b. OFFICE SYMBOL (If applicable)	9. PROCUREMENT INSTRUMENT IDENTIFICATION NUMBER: N00014-84-C-0708
3c. ADDRESS (City, State, and ZIP Code)	10. SOURCE OF FUNDING NUMBERS: PROGRAM ELEMENT NO. / PROJECT NO. / TASK NO. / WORK UNIT ACCESSION NO

11. TITLE (Include Security Classification)
Mechanism of Photon-Gated Persistent Spectral Hole-Burning in Metal-Tetrabenzoporphyrin/Halomethane Systems: Donor-Acceptor Electron Transfer

12. PERSONAL AUTHOR(S)
T. P. Carter, C. Bräuchle, V. Y. Lee, M. Manavi, and W. E. Moerner

13a. TYPE OF REPORT	13b. TIME COVERED	14. DATE OF REPORT (Year, Month, Day)	15. PAGE COUNT
Interim Technical	FROM _____ TO _____	1987,02,17	34

16. SUPPLEMENTARY NOTATION

17 COSATI CODES			18. SUBJECT TERMS (Continue on reverse if necessary and identify by block number)
FIELD	GROUP	SUB-GROUP	photon-gating, persistent spectral hole-burning, donor-acceptor electron transfer, metal-tetrabenzoporphyrin, porphyrin, halomethane

19. ABSTRACT (Continue on reverse if necessary and identify by block number)

ABSTRACT: We have observed photon-gated persistent spectral hole-burning for meso-tetra(p-tolyl)-M-tetrabenzoporphyrin (M = Zn or Mg) molecules in the presence of several different halomethanes (chloroform, methylene chloride, and methylene bromide) in poly(methyl methacrylate) thin films at liquid helium temperatures. Depending upon the sample composition and porphyrin/halomethane concentration ratio, hole formation is up to 300 times more efficient when two photons are absorbed by the porphyrin as compared to one-photon excitation. After the first (site-selecting) photon excites the singlet-singlet origin absorption near 630 nm, the most efficient photon-gating occurs when the second (gating) photon excites a strong triplet-triplet transition near 480 nm. The hole width at 1.4 K is approximately 2.5 GHz full-width at half-maximum in an inhomogeneously broadened origin absorption 300/cm in width. Analysis of the halomethane concentration dependence, the action spectrum of the second photon, the photoproduct spectrum, and the dependence of the

20. DISTRIBUTION / AVAILABILITY OF ABSTRACT: ☒ UNCLASSIFIED/UNLIMITED ☐ SAME AS RPT ☐ DTIC USERS	21. ABSTRACT SECURITY CLASSIFICATION: Unclassified
22a. NAME OF RESPONSIBLE NDIVIDUAL	22b. TELEPHONE (Include Area Code); 22c. OFFICE SYMBOL

DD FORM 1473, 84 MAR — 83 APR edition may be used until exhausted. All other editions are obsolete. — SECURITY CLASSIFICATION OF THIS PAGE

Block 19 continued

cont'd, hole depth on the time delay between the site-selecting and gating light pulses confirms that the mechanism is donor-acceptor electron transfer from an excited triplet state of the porphyrin to a nearby halomethane molecule.

OFFICE OF NAVAL RESEARCH

Contract N00014-84-C-0708

R&T Code 413a001---01

Technical Report No. 11

Mechanism of Photon-Gated Persistent Spectral Hole-Burning in Metal-Tetrabenzoporphyrin/Halomethane Systems: Donor-Acceptor Electron Transfer

by

T. P. Carter, C. Bräuchle, V. Y. Lee, M. Manavi, and W. E. Moerner

Prepared for Publication

in

Journal of Physical Chemistry

IBM Almaden Research Center
650 Harry Road
San Jose, California 95120-6099

February 17, 1987

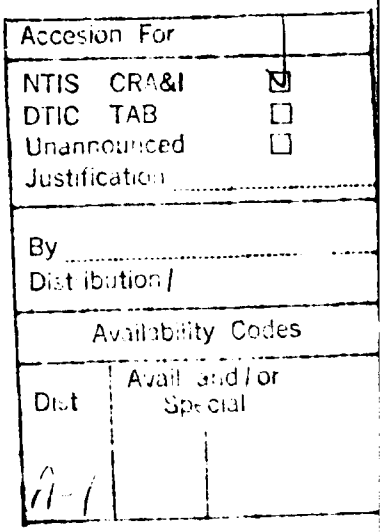

87 3

RJ 5506 (56215) 2/17/87
Chemistry

MECHANISM OF PHOTON-GATED PERSISTENT SPECTRAL HOLE BURNING IN METAL-TETRABENZOPORPHYRIN/HALOMETHANE SYSTEMS: DONOR-ACCEPTOR ELECTRON TRANSFER

T. P. Carter*
C. Bräuchle**
V. Y. Lee
M. Manavi
W. E. Moerner

IBM Almaden Research Center
San Jose, California 95120

ABSTRACT: We have observed photon-gated persistent spectral hole-burning for meso-tetra(p-tolyl)-M-tetrabenzoporphyrin (M = Zn or Mg) molecules in the presence of several different halomethanes (chloroform, methylene chloride, and methylene bromide) in poly(methyl methacrylate) thin films at liquid helium temperatures. Depending upon the sample composition and porphyrin/halomethane concentration ratio, hole formation is up to 300 times more efficient when two photons are absorbed by the porphyrin as compared to one-photon excitation. After the first (site-selecting) photon excites the singlet-singlet origin absorption near 630 nm, the most efficient photon-gating occurs when the second (gating) photon excites a strong triplet-triplet transition near 480 nm. The hole width at 1.4 K is approximately 2.5 GHz full-width at half-maximum in an inhomogeneously broadened origin absorption 300 cm^{-1} in width. Analysis of the halomethane concentration dependence, the action spectrum of the second photon, the photoproduct spectrum, and the dependence of the hole depth on the time delay between the site-selecting and gating light pulses confirms that the mechanism is donor-acceptor electron transfer from an excited triplet state of the porphyrin to a nearby halomethane molecule.

*IBM Postdoctoral Fellow
**Visiting Professor, permanent address: Institut für Physikalische Chemie der Universität München, Federal Republic of Germany

I. INTRODUCTION

The growing interest in persistent spectral hole-burning (PHB) spectroscopy is due partly to the usefulness of the PHB technique for studying low temperature photoreactions, dephasing of electronic transitions in amorphous systems, external field perturbations, and other aspects of laser spectroscopy of solids [1] [2] . In addition, PHB offers the potential for an extremely high-density optical recording technique, frequency domain optical storage [3]. While the first years of PHB research focused on single-photon mechanisms [4], the destructive reading that occurs in these systems during hole detection has generated recent interest in two-color, photon-gated materials. In photon-gating, two photons (of different wavelengths in general) are required for the photoinduced change leading to high efficiency hole-burning; only one wavelength is then required to probe the unreacted ground state population during hole detection. Beside providing a pathway to nondestructive reading, photon-gating also offers new possibilities for extremely high sensitivity in the detection of subtle perturbations due to external fields [5].

The first examples of photon-gating utilized the mechanism of two-step photoionization of the absorbing molecule or ion and subsequent trapping of the ejected electron in the nearby host matrix [6] [7] . Two-step photodissociation of photoadducts of anthracene and tetracene has also been shown to lead to photon-gating [8]. In this paper, we report the results of a mechanistic investigation of a new class of photon-gated PHB systems utilizing photo-induced donor-acceptor electron transfer (DA-ET). The specific donor molecules are derivatives of tetrabenzoporphyrin: meso-tetra(p-tolyl)-Zn-tetrabenzoporphyrin (TZT) and the magnesium analog (TMT). The acceptors are any of several halomethanes: methylene chloride,

chloroform, and methylene bromide. Previous one-color hole-burning studies of DA-ET have been performed on charge transfer complexes of Zn and Cd-porphyrins with pyridine radical anion dimers [9] [10] [11] [12] and involve transfer of an electron from the pyridine dimer to the excited metalloporphyrin. Also, two-color photochemistry has been reported in an unspecified meso-substituted Zn-tetrabenzoporphyrin in uncharacterized poly(methyl methacrylate) (PMMA), but no mechanism was suggested [13].

While we are concerned here with specific donor and acceptor molecules in PMMA thin films, we believe that the basic process is generally applicable to a variety of porphyrin-halomethane combinations in polymer matrices. Further, the goal here is to present experimental results aimed at identifying the photon-gated hole-burning mechanism, rather than to present an exhaustive account of all hole-burning properties for all donor-acceptor combinations.

To provide a framework for the experimental results to be described, Figure 1 shows a simplified level diagram for the proposed DA-ET mechanism for the porphyrin/halomethane systems of interest here. A photon at λ_1 excites the 0-0 singlet origin of the porphyrin with absorption cross-section σ_1. From the first excited singlet state S_1, the porphyrin may either relax back to the singlet ground state S_0 with rate k_f (which in general is a combination of fluorescence and internal conversion processes) or undergo intersystem crossing with rate k_{ISC} to the lowest porphyrin triplet, T_1, with a characteristically long lifetime governed by the rate k_p. Molecules which cross to the triplet manifold may then absorb a second photon at a new wavelength λ_2 with cross-section σ_2 and populate some excited triplet level, T_n. Here, the molecule may return to the lowest triplet with rate $k_{T\text{-}T}$ or transfer the excited electron to a nearby acceptor (a halomethane molecule) with rate $\eta\kappa_{T\text{-}T}$ via tunneling or other transition state mechanisms. It is this final process which leads to hole formation, since the porphyrin

cation thus generated has relatively little absorbance at λ_1. To minimize one-color hole-burning via sequential absorption of two photons of λ_1 in the singlet and triplet manifolds, it is important that there is some wavelength region where the spectral overlap of the singlet-singlet and triplet-triplet (T-T) absorption bands is minimal. In this case, the hole formed during two-color irradiation is much deeper than the hole formed by irradiation with λ_1 alone, and reading of the hole by scanning λ_1 can be quite nondestructive.

To place these DA systems in perspective compared to the larger array of DA combinations in the literature, it is instructive to estimate the equilibrium free energy release during electron transfer, ΔG, using the following relation (from Reference [14]):

$$\Delta G = F(E^D_{ox} - E^A_{red}) - E_{0,0} - \frac{e^2}{R_c \varepsilon}, \qquad (1)$$

where F is the Faraday constant, E^D_{ox} is the oxidation potential of the donor, E^A_{red} is the reduction potential of the acceptor, $E_{0,0}$ is the electronic energy deposited in the donor by the photoexcitation, e is the electronic charge, R_c is the separation distance of the ion pair, and ε is the dielectric constant of the medium. Ignoring the final term (the energy of the separated ion pair) for simplicity, and using E^D_{ox} = 0.36 eV for the unsubstituted Zn-tetrabenzoporphyrin [15] and E^A_{red} = -1.7 eV for $CHCl_3$ [16], one estimates that ΔG = -0.01 eV for excitation with λ_1 only, which is not a strong driving force. However, for two-color excitation (using a T_1 energy of 1.54 eV [17]), ΔG = -2.12 eV, which is considerably more exothermic. Thus, the DA pairs chosen for this study may be approximately regarded as combinations of fairly poor donors and acceptors that do not spontaneously undergo ET from the ground state and also do not readily undergo ET under one-color excitation. On the other hand, two-color excitation provides the donor with sufficient energy to make electron transfer far more probable, hence the photon-gating.

In this paper, we present the results of spectroscopic and hole-burning experiments which investigate the mechanism for photon-gated PHB in these metal-tetrabenzoporphyrin/halomethane/PMMA systems. We utilize the gating action spectrum for λ_2 and the photoproduct spectrum together with measurements and simulations of the gated PHB kinetics to conclude that electron ejection occurs from an upper triplet level of the porphyrin. Experiments conducted in the absence of halomethanes, together with a determination of the magnitude of the gating effect in samples with different porphyrin/halomethane concentration ratios, establish the halomethanes as the electron acceptors. Analysis of the dependence of the two-color hole depth upon the time delay between the two excitation pulses has allowed determination of the quantum efficiency for electron transfer per absorbed gating photon. A preliminary report of results for the TZT/$CHCl_3$/PMMA system has been presented [18].

II. EXPERIMENTAL

Both TZT and TMT were synthesized using a procedure similar to that described previously [19] [20] . An intimate mixture of potassium phthalimide, p-tolylacetic acid, and either zinc acetate or magnesium acetate was heated to 350-360°C under nitrogen for two hours. The resulting solid material was ground and extracted successively with hot water, petroleum ether, and chloroform. The chloroform extract was then concentrated, and the product purified by chromatography on aluminum oxide with a (1:1) chloroform/petroleum ether mixture.

The $CHCl_3$ and CH_2Cl_2 were obtained from EM Laboratories (Omnisolv, glass distilled) and used as supplied. To make sure that the non-polar hydrocarbon stabilizers used in these solvents are not responsible for the gating effect, HPLC grade $CHCl_3$ (Aldrich) containing

ethanol as stabilizer was also used; no differences in gating properties were found in samples prepared with this solvent. The CH_2Br_2 was extracted repeatedly with concentrated sulfuric acid, then washed thoroughly with water. The organic layer was dried over calcium chloride and then fractionally distilled under nitrogen.

Optical samples were prepared (under dim yellow light) by dissolving high-purity monodisperse PMMA (Polymer Laboratories $M_p \simeq 107{,}000$, $M_w/M_n < 1.10$) in the chlorinated solvent to be used as acceptor. To this solution, a small amount of either TZT or TMT was added. A few drops of the solution were placed on a pyrex, fused silica, or NaCl plate and heated to 45-75°C (depending on the acceptor) for a few minutes to drive off some of the solvent. The sample was then covered by another plate and removed from the heat. In this way, samples were formed with thickness between 50μm and 125μm. The room temperature absorption spectrum of each sample was examined, and if the optical density at the intended λ_1 was not in the range 0.3-1.0, the solution concentration was adjusted and a new sample prepared. Acceptable samples were then placed in an optical immersion cryostat already containing liquid helium at 4.2 K, in an attempt to provide reproducible cooldowns. All PHB experiments were performed at 1.4 K with the sample immersed in superfluid helium.

Figure 2 shows a schematic diagram of the experimental apparatus used to burn and probe the gated holes. A scanning, single-frequency, standing wave cw DCM dye laser (DL) with a 3 MHz linewidth was used to provide λ_1 for both burning and probing. This laser beam was not focused; the beam diameter at the sample (S) was 4 mm. A Kr^+ or Ar^+ cw ion laser was used to provide λ_2 values of 351, 413, 488, 514, 647, 676, 752, and 799 nm. This beam was expanded so that the diameter at the sample was also 4 mm. The intensities of both beams at the sample were adjusted by a combination of neutral density filters and variable attenuators (A). Sample irradiations were controlled by mechanical shutters (Sh) driven by a

combination of digital pulse and delay generators (SC), providing different irradiation times for the two colors as well as varying amounts of delay between the start of the two pulses. For reading, a signal proportional to the sample transmittance was obtained from a precision wide bandwidth (80 kHz) ratiometer (R). The denominator signal (D) was provided by a photodiode (PD) monitoring the DL intensity during the 0.25 s laser scan. The numerator signal (N) was obtained from a low-noise silicon PD monitoring the intensity after attenuation and transmission through the sample. Since the presence of a spectral hole represented a (sometimes) small change in a large signal, the ratio output was first offset to near ground potential by passing it through a precision digital voltage offset unit (O), before sending it to an averaging digital storage oscilloscope (Osc). The Osc allowed averaging of several laser scans (32, in almost all cases) to improve the signal-to-noise ratio. The digitized Osc output was then sent to a microcomputer (PC) for storage, plotting, and analysis. Not shown in Figure 2 are a wavemeter and spectrum analyzer (1.5 GHz free-spectral range) used to monitor the λ_1 frequency and stability.

A standard burn-read sequence consisted of first setting the SC for the appropriate burn times and delays, adjusting the laser intensities with closed shutters, executing the burn at a fixed λ_1 wavelength, starting the DL scan with λ_1 attenuated to the read intensity, adjusting O, and finally, acquisition on the Osc. Typical λ_1 powers (P_1) were 2 μW and 10 nW for burning and reading, respectively. The gating beam power (P_2) varied with wavelength and experimental requirements, but was usually chosen near 20 mW. For example, for λ_2 = 488 nm, the gating enhancement was largest for P_2 = 20 mW. At lower powers, the gating enhancement factor decreases presumably due to insufficient T-T excitation, whereas at higher powers shallower and broader holes are formed due to residual absorption of the gating light in the singlet manifold and subsequent sample heating. Hole depths were determined from the acquired spectra first as $\Delta T/T_1$ values, where ΔT is the final minus the initial transmittance

T_1 at the laser frequency. The $\Delta T/T_1$ values were then converted to actual hole depths $\Delta\alpha/\alpha_1$ using the approximation (valid for shallow holes)

$$\Delta\alpha/\alpha_i = (\alpha_i L)^{-1} \quad \Delta T/T_1 \quad , \tag{2}$$

where L is the sample length, α_i and α_f are the initial and final absorption coefficients at the laser frequency and $\Delta\alpha = \alpha_i - \alpha_f$. The $\Delta\alpha/\alpha_i$ values were then used for comparisons between different samples and systems.

As a representative example, the 1.4 K absorption spectrum of TMT/$CHCl_3$/PMMA is given in Figure 3. The positions and full widths at half maximum (FWHM) of the transitions in the low temperature spectra are nearly identical to those observed in room temperature spectra, attesting to a very strong inhomogeneous broadening at low temperature. In all samples, PHB experiments were performed near the peak of the $S_1 \leftarrow S_0$ origin transition of the porphyrin molecule which occurs near 633 nm for TMT and 631 nm for TZT. These spectral features lie in a region which is easily obtained with a cw single-frequency dye laser. This, together with the high molar extinction coefficient (~10^5 *l*/mole-cm) and good solubility in PMMA, makes these molecules very convenient for studying PHB processes in thin film samples.

III. RESULTS AND DISCUSSION

A. Photon Gating Characteristics

Figure 4 shows the gating enhancement effect of a second color using the TZT/$CHCl_3$/PMMA system as an example. The trace marked a) shows two holes: the shallow hole at -5 GHz (0 GHz ≡ 629.647 nm) is the result of a one-color irradiation for 6 s with

17$\mu W/cm^2$, while the deeper hole at +5 GHz is the result of identical λ_1 conditions together with simultaneous irradiation with λ_2 at 514.5 nm for 6 s with 135 mW/cm^2. Perhaps a more dramatic demonstration of the gating effect is given in trace b), which was produced similarly except that the one-color feature at -5 GHz (0 GHz ≡ 630.489 nm) was burned for 120 s. Even after this prolonged irradiation, the one-color hole depth is still only 30% of the 6 s two-color hole shown at +5 GHz.

Figure 5 shows the full-width at half-maximum (FWHM) for gated holes as a function of P_1 with constant irradiation time (6 s for both λ_1 and λ_2) at 1.4 K for the TZT/$CHCl_3$/PMMA system. For powers above 50 nW (corresponding to an intensity of 0.4 $\mu W/cm^2$) the holes show an increasing width as the power increases. Below this power, the hole width is constant at 2.54 ± 0.02 GHz under these conditions. In all samples studied, the hole widths are much broader than the lifetime limited values which may be estimated to be in the range 48-78 MHz [21] [17]). Such broadening has also been observed in other gated PHB systems involving electron ejection [6] [22] and may be due to a combination of effects: local inhomogeneous Stark shifts due to the electric fields induced by the formation of the donor-acceptor pair, reorientation of the local geometry caused by the generation of ions in the matrix [23], and/or local heating due to non-radiative relaxation processes occurring as a result of the electron transfer. Further study of the detailed mechanisms for the hole width and its temperature-dependence should be considered in future work. In particular, accumulated photon-echo measurements should be easier to perform in these photon-gated materials compared to one-color materials, because the growth of persistent holes is much slower for λ_1 excitation in the absence of λ_2.

It is helpful for purposes of comparison to define a semi-quantitative measure of the photon-gating effect. We choose to define the gating ratio, G, as the ratio of the depth of a

two-color hole to the depth of a one-color hole, for equal λ_1 irradiation times (6 s) and λ_1 burn intensities. That is, the presence of the gating radiation produces holes which are G times deeper than one-color holes using identical λ_1 conditions. Using this definition, spectrum a) of Figure 4 yields a G of 28. Values of G depend strongly on several parameters such as the particular donor-acceptor combination used, and more importantly on the acceptor-donor concentration ratio (vide infra). Representative values of G for the various systems are listed in Table I. Each value was obtained for a sample with a typical (large) acceptor-donor concentration ratio, using 6 s irradiations for both wavelengths, with $P_1 = 2\ \mu W$ and $P_2 \sim 20$ mW at $\lambda_2 = 514.5$ nm. Also included in the table are representative values of hole depth $\Delta\alpha/\alpha_1$ for each system. In general, the two-color hole depth and G values increase with increasing halo-substitution and with increasing halogen atomic weight. One possibility for this is increased triplet population due to an external heavy atom effect.

The exact values of G should not be over-interpreted because as the irradiation time is increased, the value of G changes since the growth of both one- and two-color holes is nonlinear in time. To illustrate this, the depths of one- and two-color holes as a function of irradiation time are presented in Figure 6 (note the different time scales for the two plots). As the data show, the two-color holes saturate at much shorter times than do the one-color holes. As a result, G values from experiments with long irradiation times will be lower than G values from experiments with shorter irradiation times. Perhaps a more fundamental comparison of the efficiencies for one and two-color holes can be obtained from the initial hole-burning rates, which may be measured from the initial slopes of the data in Figure 6. The ratio of these slopes yields a value of 360, which is considerably greater than the value presented in Table I; thus, the values in Table I underestimate the gating enhancement factor for shorter burn times. Nonetheless, we feel that the relative changes in G values accurately reflect the relative changes in gating enhancement from sample to sample (under identical

irradiation conditions), and for this reason we shall continue to utilize G values for the purposes of this work. The new method described above should, however, provide a more fundamental means of quantifying the gating enhancement factor for comparisons between dissimilar photon-gated PHB systems.

The role of the halomethanes as acceptors was first established by the observation that G dropped to unity (no gating) in samples prepared in their absence by using either toluene as a solvent or by heating the samples at 100 °C for several minutes to drive off all of the solvent. Further confirmation was provided by experiments in which the concentration ratio of $CHCl_3$ to TZT was quantitatively determined and compared to the G values obtained. To do this, infrared spectra were acquired over the range 600 - 700 cm^{-1} on samples which were prepared between NaCl plates, as shown in Figure 7. Trace a) shows the spectrum of a TZT/PMMA sample prepared with toluene as a solvent instead of $CHCl_3$; the peak at 700 cm^{-1} is a toluene vibrational mode. Trace b) is a spectrum of neat chloroform showing the characteristic peaks in this region, and trace c) is from an actual PHB sample ($TZT/CHCl_3/PMMA$). The peaks in c) occur at 672 cm^{-1} and 630 cm^{-1} and correspond to C-Cl stretching modes. By determining values for the molar absorptivities of these two transitions (33 *l*/mole-cm and 1.0 *l*/mole-cm, respectively), and using the published molar extinction coefficient for Zn-tetrabenzoporphyrin [24] (ϵ = 1.3 x 10^5 *l*/mole-cm), we were able to measure the chloroform/TZT concentration ratio in as-prepared hole-burning samples. The results, given in Table II, show a strong correlation between G and the $CHCl_3$/TZT ratio, which is reasonable if the acceptor is $CHCl_3$. As the donor-acceptor average separation increases with decreasing $CHCl_3$/TZT ratio, one would expect a concomitant decrease in the electron transfer probability. These results also demonstrate that the photon-gating effect depends on having large $CHCl_3$/TZT ratios (10^3 - 10^5), indicating that a relatively small fraction of $CHCl_3$ molecules are effective acceptors. This suggests that only those $CHCl_3$

molecules closest to the TZT molecule are effective acceptors. In fact, the photoreaction may also be sensitive to DA orientation, as has been suggested previously in 77 K broadband studies of ET in porphyrin-haloalkane systems [25]. Table II also illustrates the fact that G is effectively an adjustable parameter that can be controlled simply by manipulating the donor-acceptor concentration ratio - a property which can be a powerful tool for tailoring PHB systems for frequency domain optical storage applications.

B. Photon Gating Mechanism

To confirm the role of a triplet state of the porphyrin as an intermediate in the DA-ET process, the action spectrum of the gating light was determined by measuring G as a function of λ_2, using constant photon flux at every wavelength. In Figure 8 we show the results of this experiment (open circles) plotted together with the published T-T absorption spectrum for the closely related molecule Zn-tetrabenzoporphyrin (solid line)[26]. Since the gating action spectrum follows the T-T absorption fairly closely, we conclude that λ_2 is most likely absorbed by T_1 to produce the photon gating, and that the quantum yield per gating photon does not vary strongly with gating photon energy.

Further confirmation that a porphyrin T-T transition is a crucial step in the photon-gated PHB of these systems is provided by experiments in which the onset of the λ_2 pulse was delayed from the start of the λ_1 pulse. If T_1 is the intermediate level for gated hole production, the persistent hole depth should decrease with increasing delay, and the decay should reflect the lifetime of T_1, τ_T. In order to achieve reasonable temporal resolution, short (ca. 40-100 ms) λ_1 pulse-widths (irradiation times) were used in these experiments. Because of the nature of the photoreaction, the λ_2 pulse-widths were chosen to be several times longer than the triplet lifetime, to allow maximum photoreaction of the triplet population. In this

sense, the λ_2 pulse should "develop" all the triplets which are formed, to maximize the PHB yield. We have found that the decrease in hole depth with increasing delay does depend on the triplet lifetime for the TZT/$CHCl_3$/PMMA, TMT/$CHCl_3$/PMMA and TMT/CH_2Br_2/PMMA systems (the only ones studied in this manner). As an example, the results of such a delay experiment are given in Figure 9; the filled boxes represent the data for the TMT/$CHCl_3$/PMMA system.

We have also performed a series of computer simulations of the delay experiments to determine the theoretical shape of the decay curves for comparison with those experimentally obtained, as further proof of the mechanism. The curves are not simple single exponential decays because the λ_1 pulse-widths were comparable to the triplet lifetimes. For the simulations, we used the kinetic rate equations appropriate for the photophysical system depicted in Figure 1. The four coupled differential equations are:

$$\frac{dS_0}{dt} = R_1(S_1 - S_0) + k_f S_1 + k_p T_1 \tag{3}$$

$$\frac{dS_1}{dt} = -R_1(S_1 - S_0) - (k_f + k_{ISC})S_1 \tag{4}$$

$$\frac{dT_1}{dt} = R_2(T_n - T_1) + k_{ISC}S_1 + k_{T-T}T_n - k_p T_1 \tag{5}$$

$$\frac{dT_n}{dt} = -R_2(T_n - T_1) - (1 + \eta)k_{T-T}T_n \tag{6}$$

where S_0, S_1, T_1 and T_n here denote the populations of the corresponding states; R_1 and R_2 are the $S_1 \leftarrow S_0$ and $T_n \leftarrow T_1$ pumping rates, respectively; and k_f, k_p, k_{ISC}, $k_{T\text{-}T}$ and $\eta k_{T\text{-}T}$ are the rate constants for the various transitions as defined in Figure 1. (It should be noted that k_f represents the total $S_1 \rightarrow S_0$ depopulation rate: internal conversion between these states has

been shown to be negligible [21] [17] . Also, k_p represents the total depopulation rate for $T_1 \rightarrow S_0$, i. e., $k_p = 1/\tau_T$). Actual values for the pulse-widths, intensities, wavelengths and delays were included, and the coupled equations were solved using Gear's stiff integration method with full Jacobians [27]. The output consisted of the time evolution of the four states, and the final hole depth was calculated from the fraction of the population which returned to S_0 after sufficient time for all excited states to relax.

The values of all the rate constants used in the simulations are given in Table III. The k_p values were determined at low temperature using actual PHB samples by monitoring the recovery of the $S_1 \leftarrow S_0$ absorption following bleaching via pulsed dye-laser excitation into the porphyrin Soret band. Because of the large k_{ISC} values for these systems (vide infra), substantial fraction (~87% for the TZT case) of the total population could be placed into T_1 with a single laser pulse, making this method a convenient way of measuring the triplet lifetimes. The $k_{T\text{-}T}$ value was estimated from the width of the T-T spectral peak shown in Figure 8, and taken from Reference [26]. The values for the other photophysical rate constants were taken from the literature for the related molecules Zn- or Mg-tetrabenzoporphyrin as appropriate [21] [17] . The values for η, which is approximately the quantum yield per gating photon absorbed, were the only adjustable parameters and were chosen to give simulated hole depths identical to the experimental hole depths at zero delay. The results of the simulation for the TMT/$CHCl_3$/PMMA system are shown as the solid line in Figure 9, and give excellent agreement with the results of the actual PHB delay experiment. We feel that the agreement between this simulation and the experimental results, together with the measured λ_2 action spectrum, provide convincing evidence that a T-T transition is responsible for the absorption of λ_2 and, therefore, that some upper triplet level is involved in the hole formation process.

Further evidence for the proposed mechanism may be obtained from the spectrum of the PHB photoproduct. The spectrum in Figure 10, obtained from the TMT/$CHCl_3$/PMMA system, was derived by subtracting the absorption spectrum obtained after prolonged 2-color PHB over a range of λ_1's from the absorption spectrum obtained prior to hole-burning (see Figure 3). In regions where the product and educt absorbances do not overlap, new (product) absorbances appear as positive absorbance changes while lost (educt) absorbances appear as negative absorbance changes. One can see in Figure 10 that there is a loss of absorbance at all educt absorption wavelengths, indicating broadband PHB under these severe conditions. The only identifiable product absorption begins on the low energy side of the Soret band as a broad feature starting at ~500 nm, continues rising to higher energies, coming to a fairly sharp peak at ~440 nm (overlapping the strong Soret absorption of TMT), and then falling back to a featureless broad absorption below 400 nm. The dashed line in the figure shows how the TMT negative peak might look in the absence of the overlapping product absorption peak. These spectral features of the product absorption are nearly identical to the room temperature absorption of TMT^+ we obtained either through chemical oxidation by adding I_2 to a TMT/$CHCl_3$ solution after the method in Reference [28], or by two-color irradiation of a room temperature solution. Similar results were obtained for the other systems studied. Thus, in every case, we identify the chromophore photoproduct to be the porphyrin monocation. (Unfortunately, any spectral changes in the acceptor absorption lie in a region obscured by the PMMA absorption [29])

Previous one-color esr studies of the photochemistry of related Zn-porphyrins in matrices containing carbon tetrachloride or other chlorinated hydrocarbons (RCl) at 77 K [30] [31] [32] have established that the porphyrin ejects an electron which is accepted by the RCl. The acceptor then undergoes dissociative electron detachment of the form

$$e^- + RCl \rightarrow \dot{R} + Cl^-. \quad (7)$$

We therefore propose the following mechanism for the photon-gating reaction:

$$P \xrightarrow{\lambda_1, \lambda_2} P^+ + e^- \quad (8)$$

$$e^- + R' X_n \rightarrow \dot{R}' X_{n-1} + X^-. \quad (9)$$

where P is either TZT or TMT and $R'X_n$ is one of $CHCl_3$, CH_2Cl_2 or CH_2Br_2. Direct evidence for reaction 8 comes from the similarity of the porphyrin T-T absorption spectrum to the observed λ_2 action spectrum, and the measured PHB photoproduct spectrum. These data indicate sequential absorption of the two colors followed by electron ejection from an upper triplet level. Evidence for reaction 9 comes from the observations that the photon-gating effect disappears in the absence of halomethanes and that the magnitude of the effect is correlated with the $CHCl_3$/porphyrin concentration ratio, together with the analogy to previous results (reaction 7). A further indication is the absence of any observed back-reaction, even at room temperature.

C. Formation of photon-gated spectral holes on ns time scales

These DA-ET systems have some properties which make them good candidates for photon-gated PHB in a frequency domain optical storage system [33]. Two necessary properties of a practical frequency domain optical storage device are the use of small laser spots and short irradiation times (~ 30 ns), which provide for high information densities and rapid data storage and acquisition [34] [35] [36]. In order to produce detectable holes using short irradiations, the efficiency for the overall PHB process must be high since each impurity

center in the sample may absorb at most a few photons during the short burn time. As an illustration, consider a fast-burning experiment for a low efficiency system: if the overall PHB efficiency is 10^{-5} with a λ_1 pumping rate of 10^8 s^{-1}, a 30 ns irradiation will burn only about 0.003% of the centers. The relatively high overall efficiency for the systems studied in this work (~ 0.01) gives holes which are detectable using ordinary transmission spectroscopy even when burned with very short irradiation times. This high effective quantum yield is limited by the efficiency of the electron transfer step ($\eta \simeq 0.01$). However, the large values for the $S_1 \rightarrow T_1$ intersystem crossing quantum yields (0.87 for TZT, 0.45 for TMT; see Table III) enable total bleaching of the sample at λ_1 with a 30 ns pulse using reasonable (mW) power levels. Also, the long triplet lifetimes (see Table III) provide for relatively long λ_2 irradiations. This allows a center to undergo multiple λ_2 excitations thus increasing the overall yield for the process even with very short λ_1 irradiations.

To give an experimental example, Figure 11 shows a hole burned in TZT/$CHCl_3$/PMMA with 10 mW from the cw dye laser focused to a 200 μm diameter spot with a single 30 ns pulse (produced by an acousto-optic modulator with contrast ratio greater than 10000:1). The gating was provided by a simultaneous unfocused 200 ms pulse at 488 nm with 19 mW. Figure 11(a) is the baseline before burning; trace 11(b) shows a hole burned by the single 30 ns irradiation. Attempts to produce a measurable one-color hole using these conditions were unsuccessful. Thus, the overall PHB efficiency of these materials is high enough to produce easily detectable holes in small spots with very short λ_1 irradiation times. The long duration of the λ_2 pulse should not be considered a drawback; the large τ_T for these systems allows for many different λ_1 pulses to be applied to the sample to put selected groups of donor molecules in T_1. All such molecules can then be "developed" by a single λ_2 irradiation, thereby amortizing the long λ_2 time over the production of many holes. Due to the photon-gating property, the high efficiency, and the ability to vary the gating characteristics by varying the

acceptor concentration and electron affinity, this class of systems exhibits several of the properties needed for a practical frequency-domain optical storage medium, and provides an impetus for further study of DA-ET systems, including linked donor-acceptor molecules [37] that might provide improved reversibility.

ACKNOWLEDGEMENT

This work was supported in part by the U.S. Office of Naval Research.

Table I. Typical Photon Gating Characteristics

System	G	$\Delta\alpha/\alpha_i$
TZT/$CHCl_3$/PMMA	5 - > 30	0.1 - 0.3
TZT/CH_2Cl_2/PMMA	4	0.05 - 0.08
TZT/CH_2Br_2/PMMA	10 - 15	0.2 - 0.3
TMT/$CHCl_3$/PMMA	40	0.2
TMT/CH_2Br_2/PMMA	13	0.2

Table II. Dependence of Gating on Donor-Acceptor Concentration Ratio

[TZT] (10^{-5} M)	[$CHCl_3$] (M)	$\frac{[CHCl_3]}{[TZT]}$	G
99	2.8	2.8×10^3	5.4
68	10	1.5×10^4	19
9.6	9.4	9.8×10^4	> 30

Table III. Photophysical Rates for the Various Systems

	TZT			TMT	
	$CHCl_3$	CH_2Cl_2	CH_2Br_2	$CHCl_3$	CH_2Br_2
k_f $(10^6\ s^{-1})^a$	50.0			83.5	
k_{ISC} $(10^6\ s^{-1})^a$	342			68.3	
k_{T-T} $(10^{14}\ s^{-1})^b$	3.20				
k_p (s^{-1})	25.7	21.4	86.2	9.09	29.03
η	0.0346	–	–	0.0143	0.0067

REFERENCES

1. J. Friedrich and D. Haarer, Angew. Chem. Int. Ed. Engl. 23, 113 (1984).
2. G. J. Small, in Spectroscopy and Excitation Dynamics of Condensed Molecular Systems, ed. by V. M. Agranovitch and R. M. Hochstrasser, (North-Holland, Amsterdam 1983), pp. 515-554.
3. G. Castro, D. Haarer, R. M. Macfarlane, and H. P. Trommsdorff, "Frequency selective optical data storage system," U. S. Patent No. 4,101,976, (1978).
4. W. E. Moerner and M. D. Levenson, J. Opt. Soc. Amer. B: Optical Physics 2, 915 (1985).
5. R. M. Macfarlane, R. M. Shelby and A. Winnacker, Phys. Rev. B 33, 4207 (1986).
6. A. Winnacker, R. M. Shelby, and R. M. Macfarlane, Opt. Lett. 10, 350 (1985).
7. H. W. H. Lee, M. Gehrtz, E. E. Marinero, and W. E. Moerner, Chem. Phys. Lett. 118, 611 (1985).
8. M. Iannone, G. W. Scott, D. Brinza, and D. R. Coulter, J. Chem. Phys. 85, 4863 (1986).
9. V. G. Maslov, Opt. Spektrosk. 51, 1009 (1981).
10. V. G. Maslov, Opt. Spektrosk. 45, 1019 (1978).
11. V. G. Maslov, Opt. Spektrosk. 45, 824 (1978).
12. V. G. Maslov, Opt. Spektrosk. 43, 388 (1977).
13. O. N. Korotaev, E. I. Donskoi, and V. I. Glyadkovskii, Opt. Spektrosk. 59, 492 (1985).
14. J. W. Verhoeven, Pure Appl. Chem. 58, 1285 (1986).
15. A. Vogler, B. Rethwisch, H. Kunkley, J. Huttermann, and J. O. Besenhard, Angew. Chem. Int. Ed. Engl. 17, 951 (1978).
16. A. J. Bard, ed., Encyclopedia of Electrochemistry of the Elements, Vol. XIV, (Marcel Dekker, New York, 1978), p. 27.
17. A. T. Gradyushko and M. P. Tsvirko, Opt. Spektrosk. 31, 291 (1971).

18. T. P. Carter, C. Brauchle, V. Y. Lee, M. Manavi, and W. E. Moerner, (Optics Letters, to appear).

19. V. N. Kopranenkov, S. N. Dashkevich, and E. Ya. Lukyanets, Zh. Obshch. Khim. 51, 2513 (1981).

20. V. N. Kopranenkov, E. A. Makarova, and E. A. Luk'yanets, Zh. Obshch. Khim. 51, 2727 (1981).

21. A. T. Gradyushko, A. N. Sevchenko, K. N. Solovyov, and M. P. Tsvirko, Photochem. Photobiol. 11, 387 (1970).

22. R. M. Macfarlane and J. C. Vial, Phys. Rev. B 34, 1 (1986).

23. F. C. Bos and J. Schmidt, J. Chem. Phys. 84, 584 (1986).

24. M. Gouterman, J. Mol. Spectrosc. 6, 138 (1961).

25. L. N. Strekova, E. Kh. Brikenshtein, A. N. Asanov, N. A. Sadovskii, and R. F. Khairutdinov, Izv. Acad. Nauk SSSR, Ser. Khim. 6, 1227 (1981).

26. M. P. Tsvirko, V. V. Sapunov, and K. N. Solovev, Opt. Spektrosk. 34, 1094 (1973).

27. Digital Simulation Language / VS, IBM Program Number 5798-PXJ.

28. J. C. Goedheer, Photochem. Photobiol. 6, 521 (1967).

29. C. R. Zobel and A. B. F. Duncan, J. Am. Chem. Soc. 77, 2611 (1955).

30. R. F. Khairutdinov, E. K. Brickenstein, and L. N. Strekova, Izv. Akad. Nauk SSSR, Ser. Khim. 7, 1504 (1982).

31. Z. Gasyna, W. R. Browett, and M. J. Stillman, Inorg. Chim. Acta 92, 37 (1984).

32. E. K. Brickenstein, G. K. Ivanov, M. A. Kozhushner, and R. F. Khairutdinov, Chem. Phys. 91, 133 (1984).

33. W. E. Moerner, T. P. Carter, and C. Brauchle, (to appear in Appl. Phys. Lett., February, 1987).

34. W. E. Moerner, J. Molec. Elec., 1, 55 (1985).

35. M. Romagnoli, W. E. Moerner, F. M. Schellenberg, M. D. Levenson, and G. C. Bjorklund, J. Opt. Soc. Am. B: Opt. Phys. 1, 341 (1984).

36. W. Lenth and W. E. Moerner, Opt. Commun. 58, 249 (1986).

37. N. S. Hush, M. N. Paddon-Row, E. Cotsaris, H. Oevering, J. W. Verhoeven, and M. Heppener, Chem. Phys. Lett. 117, 8 (1985).

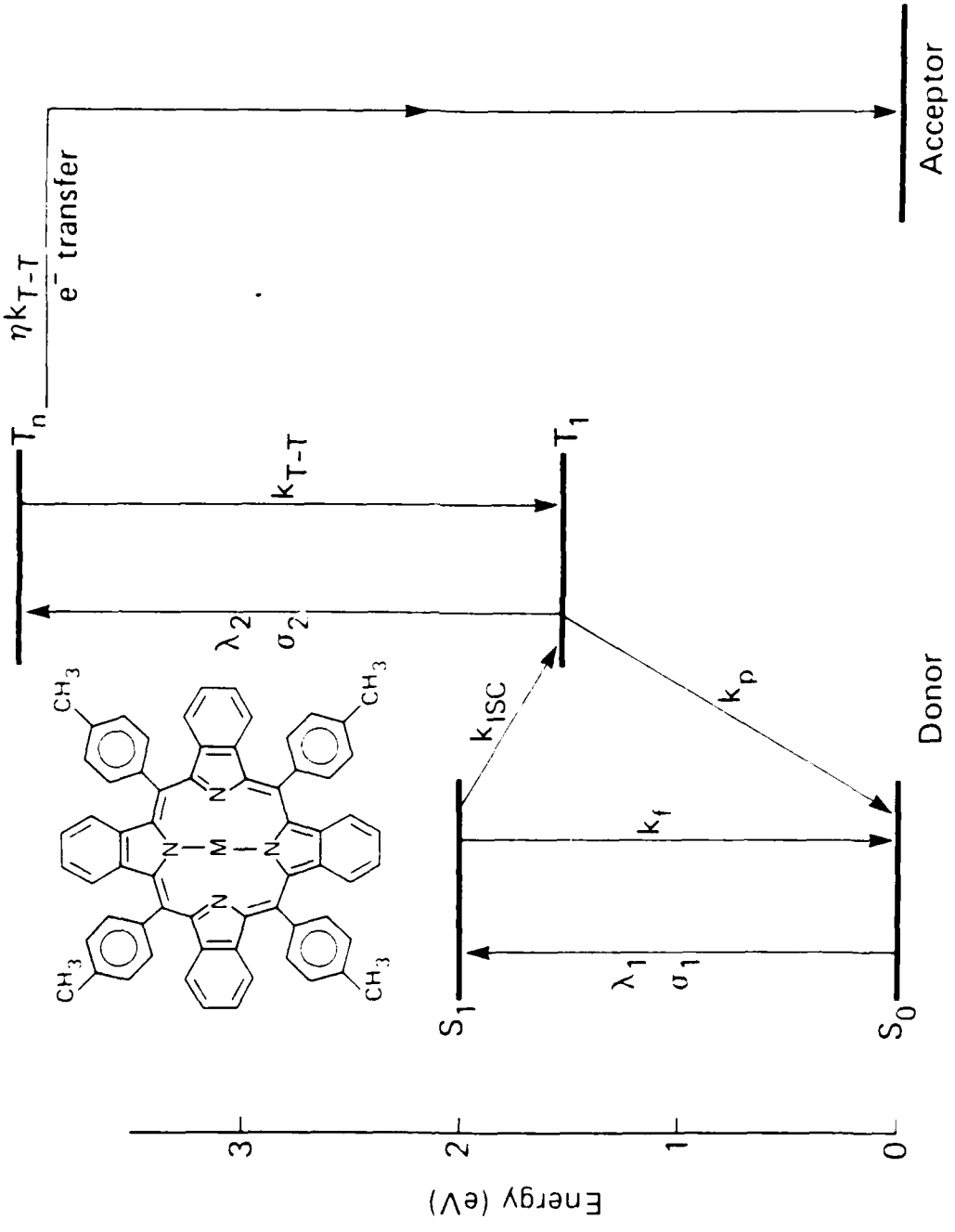

Figure 1. Level diagram for photon-gated PHB via DA-ET. The structure of the donor molecule is shown in the inset, where M denotes either Zn(II) or Mg(II). The k's denote the rate constants for the indicated transitions: σ_1 and σ_2 are the absorption cross-sections at λ_1 and λ_2, respectively.

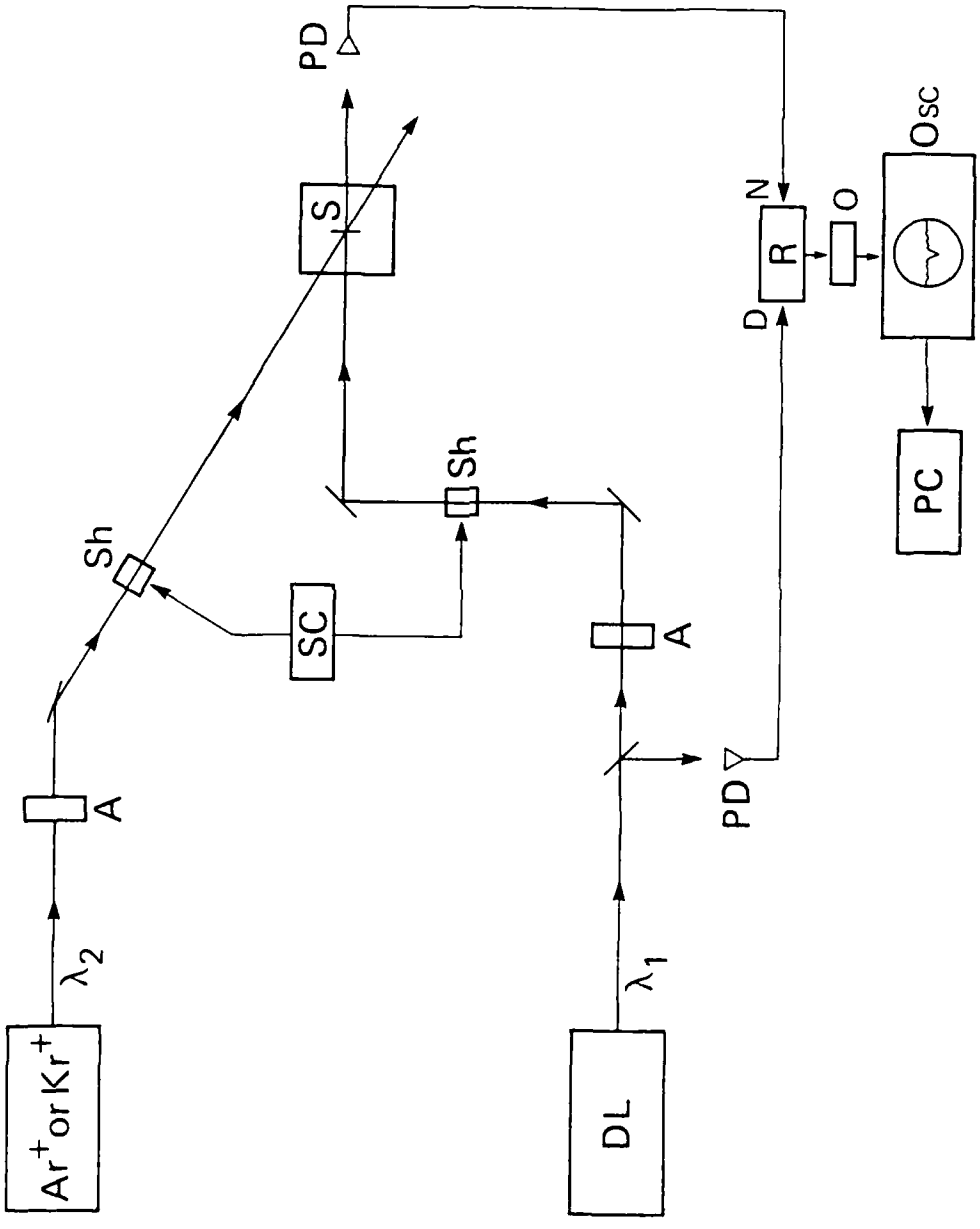

Figure 2. Schematic diagram of PHB apparatus. Legend: DL - dye laser providing λ_1, A - neutral density filters/variable attenuator, Sh - mechanical shutters, SC - shutter controllers, Ar^+ or Kr^+ - ion lasers providing λ_2, S - sample in cryostat, PD - silicon photodetectors, R - precision ratiometer, O - precision digital offsetter, Osc - digital storage oscilloscope, PC - microcomputer.

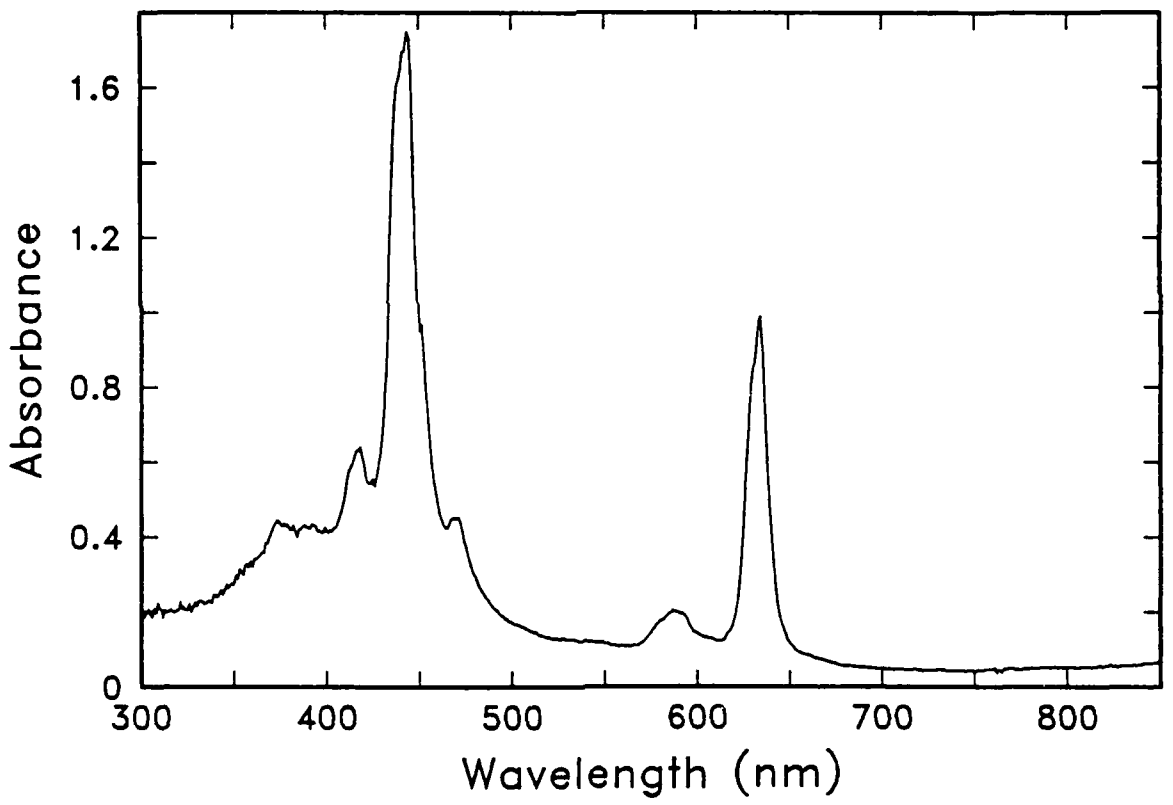

Figure 3. Low temperature absorption spectrum of TMT/$CHCl_3$/PMMA.

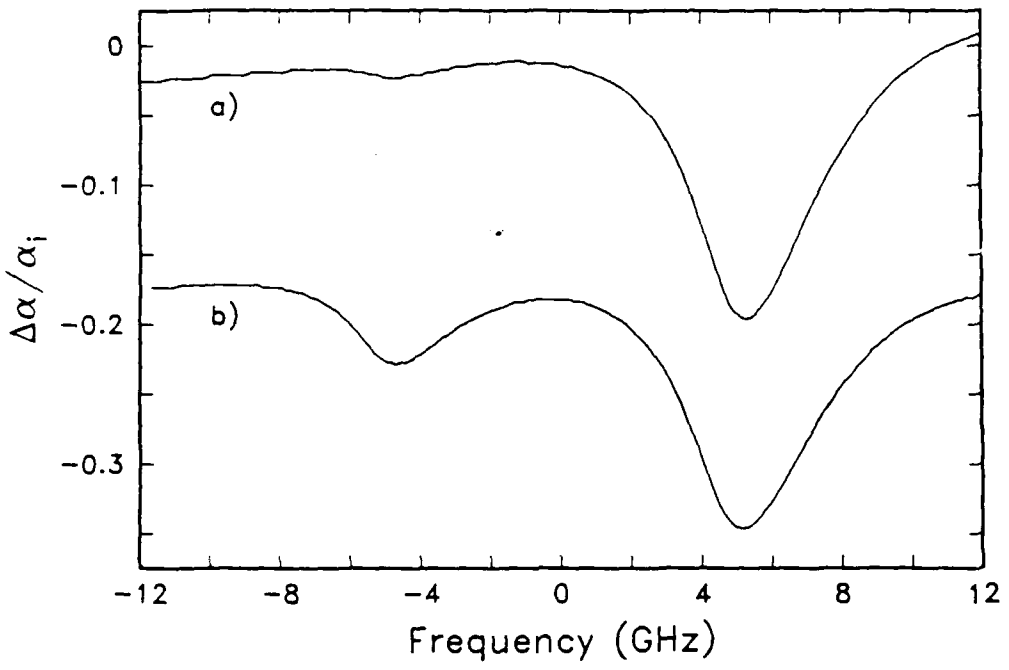

Figure 4. Photon-gated PHB in TZT/$CHCl_3$/PMMA. Trace a) shows two holes: the shallow hole at -5 GHz (0 GHz = 629.6 nm) resulted from a one-color irradiation only (6 s, 17μW/cm^2); the deeper hole at +5 GHz resulted from identical λ_1 conditions together with simultaneous irradiation with λ_2 (6 s, 135 mW/cm^2, 514.5 nm). Trace b) was produced similarly except that the one-color feature at -5 GHz (0 GHz = 630.5 nm) was burned for 120 s.

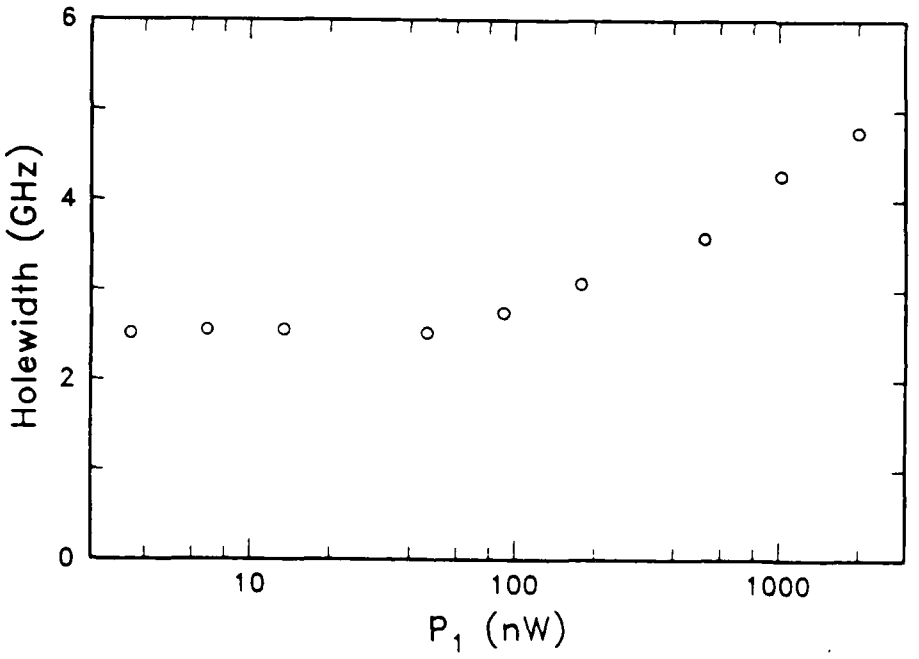

Figure 5. Hole width vs. λ_1 burn power at constant λ_1 and λ_2 irradiation times (6 s each, λ_2 = 488 nm, P_2 = 19 mW) for photon-gated holes in TZT/$CHCl_3$/PMMA.

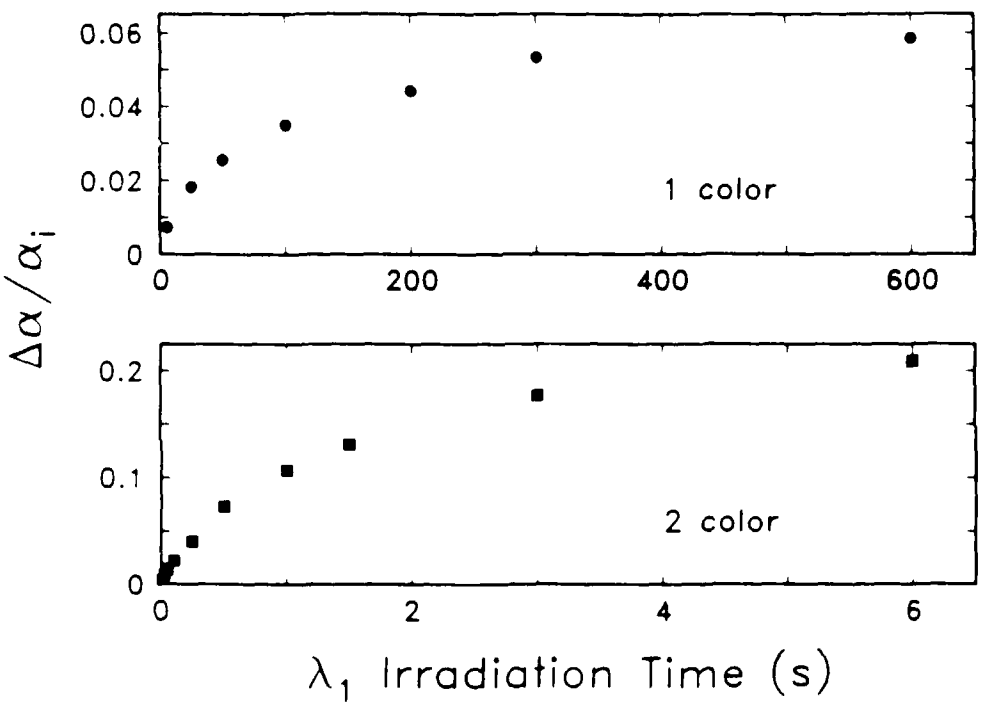

Figure 6. One and two-color hole depth vs. λ_1 irradiation time with constant power in the TZT/$CHCl_3$/PMMA system. The top panel shows the hole growth for one-color holes; the λ_1 power was 2 μW corresponding to an intensity of 16 $\mu W \cdot cm^{-2}$. The initial slope of the data points is 1.22×10^{-3} s^{-1}. The lower panel shows the two-color hole depth vs. λ_1 irradiation time with constant P1 and P2 (2 μW and 19 mW, respectively). The λ_2 irradiation time was equal to that for λ_1 for irradiations of 250 ms or more but was kept at 250 ms for shorter λ_1 irradiations. The initial slope of the data points is 0.441 s^{-1}.

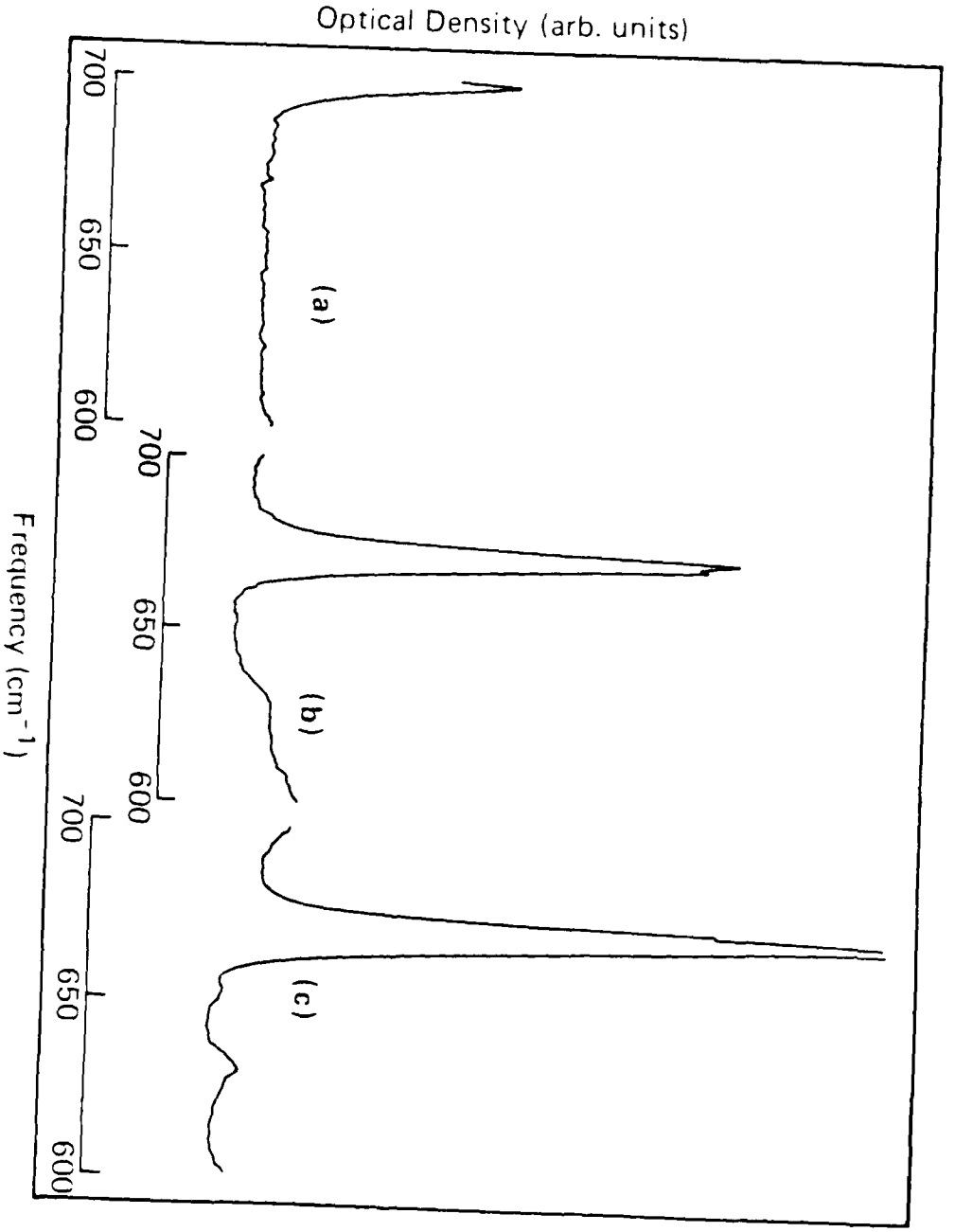

Figure 7. Room temperature IR spectrum of $CHCl_3$ vibrational modes over the range 600-700 cm^{-1}. Trace a) shows a TZT/PMMA sample prepared with toluene instead of $CHCl_3$; trace b) is the spectrum of neat $CHCl_3$; trace c) is from a TZT/$CHCl_3$/PMMA sample.

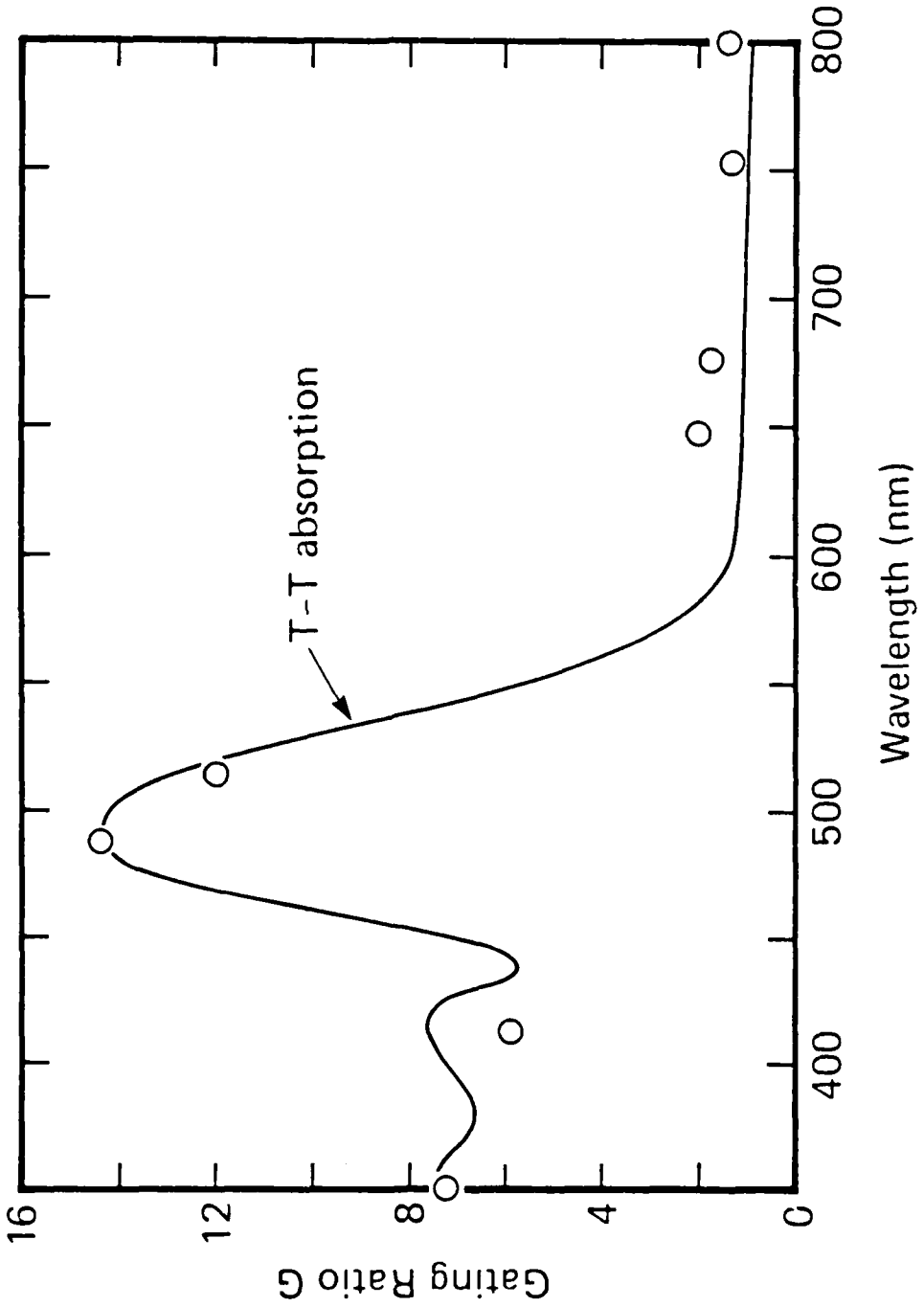

Figure 8. Photon-gating action spectrum for λ_2 in TZT/$CHCl_3$/PMMA (open circles). The solid line represents the T-T absorption spectrum of the closely related molecule Zn-tetrabenzoporphyrin, taken from Ref. [26].

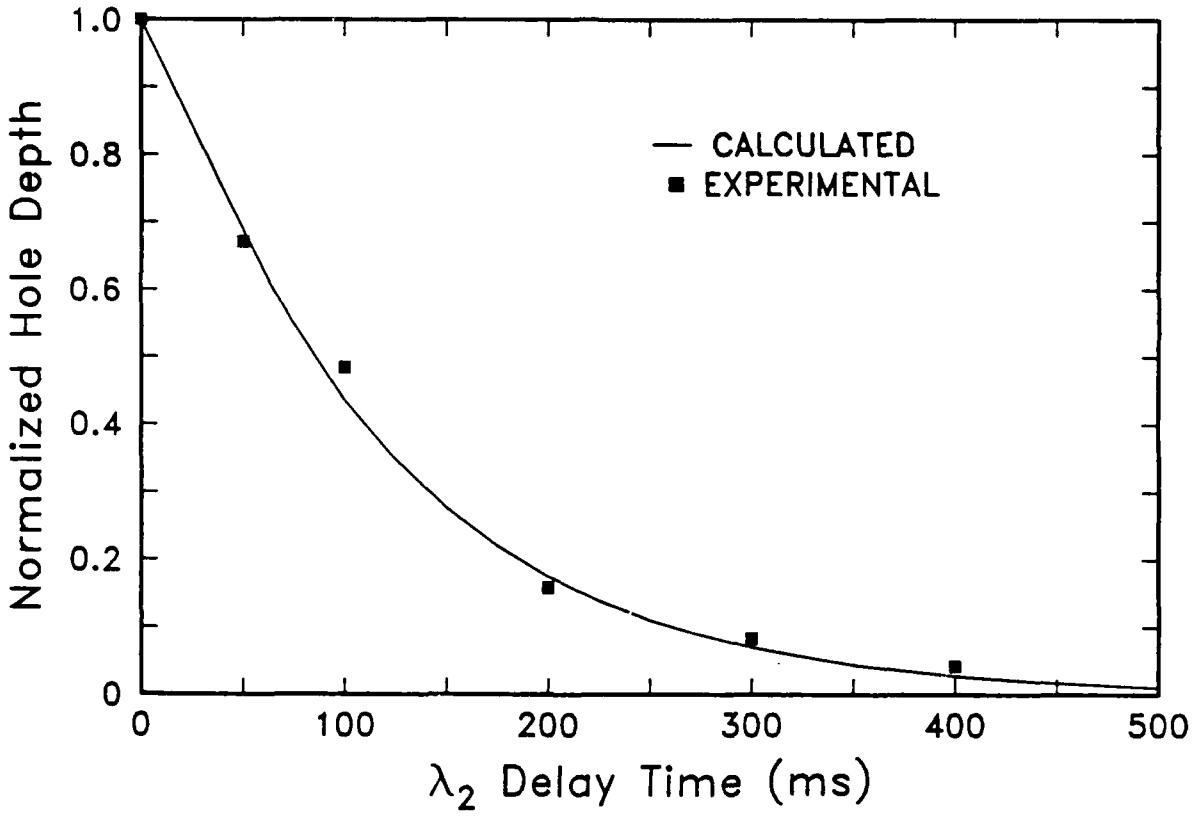

Figure 9. Photon-gated hole depth as a function of λ_2 delay for TMT/$CHCl_3$/PMMA. The filled boxes represent the results of the two-color PHB experiments; the solid line was generated from a series of delay simulations using the kinetic equations for the photophysical system depicted in Figure 1 and the parameters listed in Table III.

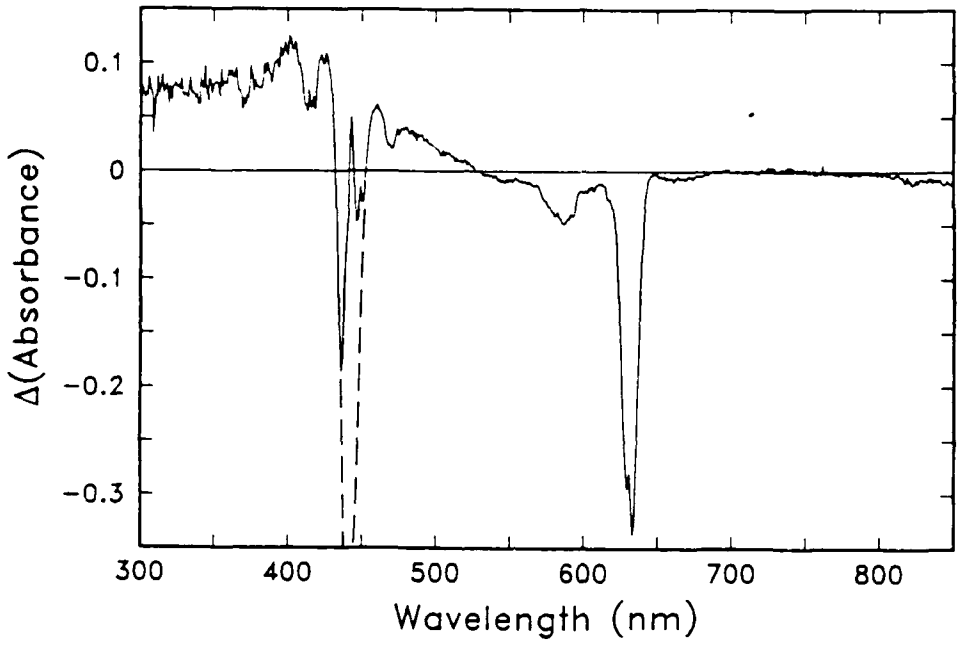

Figure 10. Low temperature PHB product spectrum for TMT/$CHCl_3$/PMMA obtained by subtracting an unburned absorption spectrum from one taken after extensive photon-gated PHB. Downward transitions represent a loss of the original absorption. Upward transitions correspond to the absorption of the PHB photoproduct; the only strong peak of this type occurs nearly at the center of the TMT absorbance at ~440 nm. The dashed line shows how the TMT negative peak might look in the absence of this product absorption.

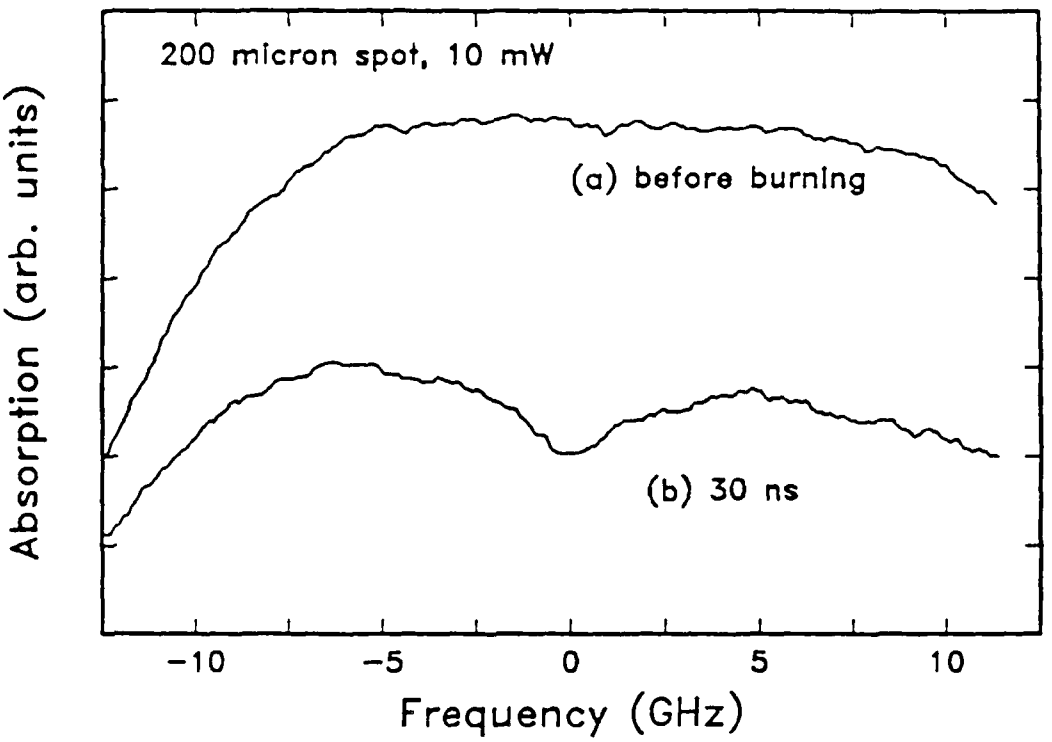

Figure 11. Short-pulse, small-spot photon-gated hole burning in TZT/$CHCl_3$/PMMA. Trace a) shows the spectrum before burning; trace b) shows a hole burned using a single 30 ns λ_1 pulse (10 mW peak power) focused to a 200 μm diameter spot together with an unfocused (0.4 cm diameter) λ_2 pulse at 488 nm for 200 ms with 19 mW. The curvature in the two spectra is repeatable and due to weak Fabry-Perot resonances in the optical system. The hole depth corresponds to approximately a 1% change in transmittance.

TECHNICAL REPORT DISTRIBUTION LIST, GEN

	No. Copies
Office of Naval Research Attn: Code 1113 800 N. Quincy Street Arlington, Virginia 22217-5000	2
Dr. Bernard Douda Naval Weapons Support Center Code 50C Crane, Indiana 47522-5050	1
Naval Civil Engineering Laboratory Attn: Dr. R. W. Drisko, Code L52 Port Hueneme, California 93401	1
Defense Technical Information Center Building 5, Cameron Station Alexandria, Virginia 22314	12 high quality
DTNSRDC Attn: Dr. H. Singerman Applied Chemistry Division Annapolis, Maryland 21401	1
Dr. William Tolles Superintendent Chemistry Division, Code 6100 Naval Research Laboratory Washington, D.C. 20375-5000	1
Dr. David Young Code 334 NORDA NSTL, Mississippi 39529	1
Naval Weapons Center Attn: Dr. Ron Atkins Chemistry Division China Lake, California 93555	1
Scientific Advisor Commandant of the Marine Corps Code RD-1 Washington, D.C. 20380	1
U.S. Army Research Office Attn: CRD-AA-IP P.O. Box 12211 Research Triangle Park, NC 27709	1
Mr. John Boyle Materials Branch Naval Ship Engineering Center Philadelphia, Pennsylvania 19112	1
Naval Ocean Systems Center Attn: Dr. S. Yamamoto Marine Sciences Division San Diego, California 91232	1

TECHNICAL REPORT DISTRIBUTION LIST, 051A

Dr. M. A. El-Sayed
Department of Chemistry
University of California
Los Angeles, California 90024

Dr. E. R. Bernstein
Department of Chemistry
Colorado State University
Fort Collins, Colorado 80521

Dr. J. R. MacDonald
Chemistry Division
Naval Research Laboratory
Code 6110
Washington, D.C. 20375-5000

Dr. G. B. Schuster
Chemistry Department
University of Illinois
Urbana, Illinois 61801

Dr. J.B. Halpern
Department of Chemistry
Howard University
Washington, D.C. 20059

Dr. M. S. Wrighton
Department of Chemistry
Massachusetts Institute of Technology
Cambridge, Massachusetts 02139

Dr. A. Paul Schaap
Department of Chemistry
Wayne State University
Detroit, Michigan 49207

Dr. W.E. Moerner
I.B.M. Corporation
Almaden Research Center
650 Harry Rd.
San Jose, California 95120-6099

Dr. A.B.P. Lever
Department of Chemistry
York University
Downsview, Ontario
CANADA M3J1P3

Dr. John Cooper
Code 6173
Naval Research Laboratory
Washington, D.C. 20375-5000

Dr. George E. Walrafen
Department of Chemistry
Howard University
Washington, D.C. 20059

Dr. Joe Brandelik
AFWAL/AADO-1
Wright Patterson AFB
Fairborn, Ohio 45433

Dr. Carmen Ortiz
Consejo Superior de
Investigaciones Cientificas
Serrano 121
Madrid 6, SPAIN

Dr. John J. Wright
Physics Department
University of New Hampshire
Durham, New Hampshire 03824

Dr. Kent R. Wilson
Chemistry Department
University of California
La Jolla, California 92093

Dr. G. A. Crosby
Chemistry Department
Washington State University
Pullman, Washington 99164

Dr. Theodore Pavlopoulos
NOSC
Code 521
San Diego, California 91232

END

4-87

DTIC